Synthesis, Structure and Characterisation of New Phenolato-Bridged Manganese Complexes $[L_2Mn_2]^{2+}$ − Formation by Ligand Oxidation in L_aH [L_aH = *N*-(2-hydroxybenzyl)-*N*,*N*′-bis(2-pyridylmethyl)ethane-1,2-diamine]

Christelle Hureau,[a] Elodie Anxolabéhère-Mallart,[a] Martine Nierlich,[b] Florence Gonnet,[d] Eric Rivière,[a] and Geneviève Blondin*[a]

Keywords: Manganese / N,O ligands / Electrochemistry / EPR spectroscopy

A mononuclear $[L_aMn^{III}OAc](ClO_4)\cdot 0.5H_2O$ [**2**$(ClO_4)\cdot 0.5H_2O$] complex with a new amino-containing pentadentate ligand L_aH with a $[N_4O]$ coordination sphere has been obtained. Magnetic susceptibility measurements of **2**$(ClO_4)\cdot 0.5H_2O$ indicated a high spin electronic configuration for the Mn^{III} ion. In cyclic voltammetry the reversible wave observed at $E_{1/2}$ = 0.15 V vs. SCE was attributed to the reduction of Mn^{III} into Mn^{II}. In acetonitrile solution complex **2** spontaneously evolved into phenolato-bridged $Mn^{II}Mn^{II}$ dimeric complexes with the concomitant oxidation of the ligand. X-ray diffraction structures revealed that there is indeed a 1:1 mixture of two closely related complexes: in one case both ligands L_a^- have been oxidised to the imine form leading to the $[L_iMn^{II}Mn^{II}L_i]^{2+}$ cation (**1a**), whereas in the other, only one ligand has been oxidised, leading to the $[L_aMn^{II}Mn^{II}L_i]^{2+}$ cation (**1b**). In both **1a** and **1b**, Mn^{II} ions are in a distorted octahedral environment. Crystallographic data indicated that the Mn_2O_2 core is similar for **1a** and **1b.** The complete spectroscopic and electrochemical studies performed on powder samples and on acetonitrile solutions did not allow one to distinguish between the two cations. The magnetic susceptibility measurements performed on a powder sample of **1**$(BPh_4)_2\cdot 2CH_3COCH_3$ was characteristic of a weak antiferromagnetic coupling interaction between the two high-spin Mn^{II} ions (g = 1.95 and J = –1.5 cm^{-1}). Similar behaviour was observed for the powder sample of **1**$(ClO_4)_2\cdot H_2O$ (g = 1.96 and J = –2.9 cm^{-1}). Powder samples of **1**$(BPh_4)_2\cdot 2CH_3COCH_3$ and **1**$(ClO_4)_2\cdot H_2O$ showed EPR intensity variations with temperature indicating that the signal was mainly due to the S = 2 spin state. EPR spectra run on the acetonitrile solutions indicated that the dinuclear structure of **1** is maintained. In cyclic voltammetry, complex **1**$(ClO_4)_2\cdot H_2O$ exhibited a quasi-reversible wave in oxidation at E_p = 0.71 V vs. SCE, attributed to the slow electron transfer of the $Mn^{II}Mn^{II}/Mn^{II}Mn^{III}$ redox process ($k_s^{app} = 1.10^{-4}$ $cm^2\cdot s^{-1}$).

Introduction

Manganese is involved in several essential processes of life.[1] One famous example is the oxidation, under light, of water into dioxygen that is catalysed by the tetranuclear (oxo)Mn cluster of the Oxygen Evolving Complex (OEC) located in the photosystem II of green plants.[2,3] Dinuclear manganese clusters are present in several metalloproteins.[4,5] Among them, one can quote the manganese catalases, arginase and manganese ribonucleotide reductase.

In the last decade, X-ray diffraction studies were performed on an increasing number of metalloproteins, allowing new insight into the active sites. Resolution may, however, not be sufficient to predict either, the nature of the ligands[6] or the spatial arrangement of the metal ions.[7,8] The determination of the nature of the active sites still relies on the analysis of spectroscopic data. For instance, different hypotheses are formulated for the Mn_4 cluster of the OEC based on X-ray absorption investigations in conjunction with electronic spin resonance techniques (EPR, ENDOR, ESEEM).[3,9−11] Another example is the magnetisation studies run on catalases.[12]

Synthesising new complexes is still a challenge for the chemists along with the investigation of spectroscopic characteristics of such molecules and the perspective of elaborating new catalysts.

[a] Laboratoire de Chimie Inorganique, UMR 8613, Institut de Chimie Moléculaire d'Orsay, Université Paris-Sud, 91405 Orsay Cedex, France
Fax: (internat.) + 33-1/69154754
E mail: gblondin@icmo.u-psud.fr
[b] CEA Saclay, DRECAM/SCM Bat 125, 91191 Gif-Sur-Yvette, France
[c] Laboratoire de Chimie Structurale Organique et Biologique, Université Pierre et Marie Curie, 75005 Paris, France
[d] Present address: Laboratoire Analyse et Environnement, UMR 8587, Bâtiment des Sciences, Université d'Evry Val d'Essonne, Boulevard François Mitterrand, 91025 Evry Cedex, France

Supporting information for this article is available on the WWW under http://www.eurjic.org or from the author.

In relation to the OEC, we are interested in the EPR signatures of mixed-valent dinuclear $Mn^{III}Mn^{IV}$ systems for which the chemical nature of the bridge appears to have a great influence on the EPR signature. At the X-band, both the $[Mn^{III}-(\mu\text{-}O)_2-Mn^{IV}]^{3+}$ [13,14] and $[Mn^{III}-(\mu\text{-}O)_2(\mu\text{-}OAc)-Mn^{IV}]^{2+}$ [15,16] core systems present 16-line spectra that differ in their relative line intensities while the only mono(μ-oxo) complex reported in the literature, $[L'_iMn^{III}-(\mu\text{-}O)-Mn^{IV}L'_i]^{3+}$ (see Scheme 1), exhibits a peculiar 18-line spectrum.[17] In order to synthesise a new $Mn^{III}-(\mu\text{-}O)-Mn^{IV}$ system, we designed a ligand very similar to the one (L'_iH) used by Horner et al. In the laboratory, we previously used these ligands in the amine form (noted L_aH and L'_aH in Scheme 1) to synthesise $Fe^{III}-(\mu\text{-}O)-Fe^{III}$ systems and found that both ligands behave the same.[18,19] We will show here that this is not the case when the trivalent metal used is manganese. Following the same synthetic route reported for the formation of $[L'_iMn^{III}-(\mu\text{-}O)-Mn^{III}L'_i]^{2+}$, a mononuclear Mn^{III} complex is isolated when ligand L_aH is used instead of L'_aH. We found that this complex evolves into a bis(μ-phenolato)bis(Mn^{II}) complex with the concomitant dehydrogenation of the amine function of the ligand. Only three out of four ligands are indeed oxidised and we will designate LH to the mixture of L_aH and L_iH present in the isolated dinuclear Mn^{II} complex.

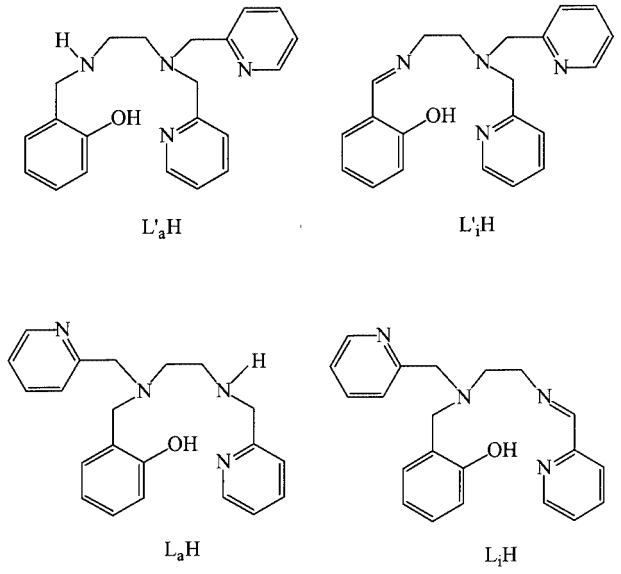

Scheme 1

Results and Discussion

Starting from $Mn(OAc)_3{\cdot}nH_2O$ and the ligand L_aH, a mononuclear Mn^{III} complex **2** was isolated as a perchlorate salt. No X-ray structure could be obtained, but the entire characterisation allows us to propose the formula $[L_aMnOAc]^+$ for **2**, which is in good agreement with all the measurements that were taken. Complex **2** evolves spontaneously in solution and leads to the formation of the dinuclear Mn^{II} complex **1** that was isolated using BPh_4^- or ClO_4^-. The two powdered samples $[\mathbf{1}](BPh_4)_2{\cdot}2CH_3COCH_3$ and $[\mathbf{1}](ClO_4)_2{\cdot}H_2O$ were characterised. Crystals were only obtained with tetraphenylborate as a counterion. Based on the whole characterisation of $[\mathbf{1}](BPh_4)_2{\cdot}2CH_3COCH_3$ and $[\mathbf{1}](ClO_4)_2{\cdot}H_2O$ discussed below, it is shown that the cation is the same in the two complexes. The dehydrogenation of the secondary amine which goes with the conversion of **2** into **1** is corroborated by the IR spectra. The vibration detected at 1665 cm^{-1} for $[\mathbf{1}](BPh_4)_2{\cdot}2CH_3COCH_3$ or 1661 cm^{-1} for $[\mathbf{1}](ClO_4)_2{\cdot}H_2O$ may be assigned to a coordinated imine function. No such vibration is detected for **2** indicating that the ligand remains as introduced.

X-ray Crystal Structure of $[L_2Mn_2](BPh_4)_2{\cdot}2CH_3COCH_3$

The structure consists of one $[LMn^{II}Mn^{II}L]^{2+}$ complex cation, two tetraphenylborate anions and two acetone molecules. The structure reveals that the complex is indeed a mixture of two closely related complexes in a 1:1 ratio. In complex **1a**, both ligands have been oxidised and exhibit an imine function conjugated to one pyridine group in place of the secondary amine function present in L_a^-. In complex **1b**, only one ligand has been oxidised while the second is the unchanged amine. A view of the cations is presented in Figure 1 and selected bond lengths and angles are listed in Table 1.

In both cations **1a** and **1b**, the two manganese ions are coordinated by the four nitrogen atoms of one ligand and by two oxygen atoms from phenolato groups, one belonging to the same ligand, and the other to the ligand coordinating the other metallic site. The metallic ions in **1a** and **1b** are in a distorted octahedral environment as shown by the angle values listed in Table 1. Such angle values are commonly observed in hexacoordinated Mn^{II} complexes.

The imine function is identified by the short C24−N6 and C3A−N2A bond lengths [1.310 (8) Å and 1.32 (2) Å] in the ligand coordinated to the Mn2 and Mn1 sites respectively. Moreover, the sum of the angles around the nitrogen atoms N6 or N2A approaches 360° (351° around N6, 343° around N2A), clearly demonstrating the sp^2 hybridisation of the nitrogen atoms.

The $Mn^{II}-N$ bond lengths in **1a** and **1b** are close to the values commonly observed for Mn^{II} complexes[20−26] except for the Mn1−N2A distance (2.375 Å) in **1a**. This distance is longer than the observed $Mn^{II}-N$ bond lengths (2.20−2.32 Å) where the nitrogen atom belongs to a phenolate conjugated imine function.[27−29]

The Mn2 moiety is common to the cations **1a** and **1b**. A comparison of the Mn1 moieties is shown in Figure 2. The folding of the ligand L_i^- around the metal centre is the same for Mn1 and Mn2 in complex **1a**, but the folding of the ligand L_a^- is not the same, leading to a different environment around the Mn1 atom in **1b**: (i) the phenolate ring planes are almost orthogonal (81°), (ii) the tertiary amine nitrogen atom to which this phenolate group is linked (N1A in **1a** and N1B in **1b**) is *cis* to the bridging phenolate O2

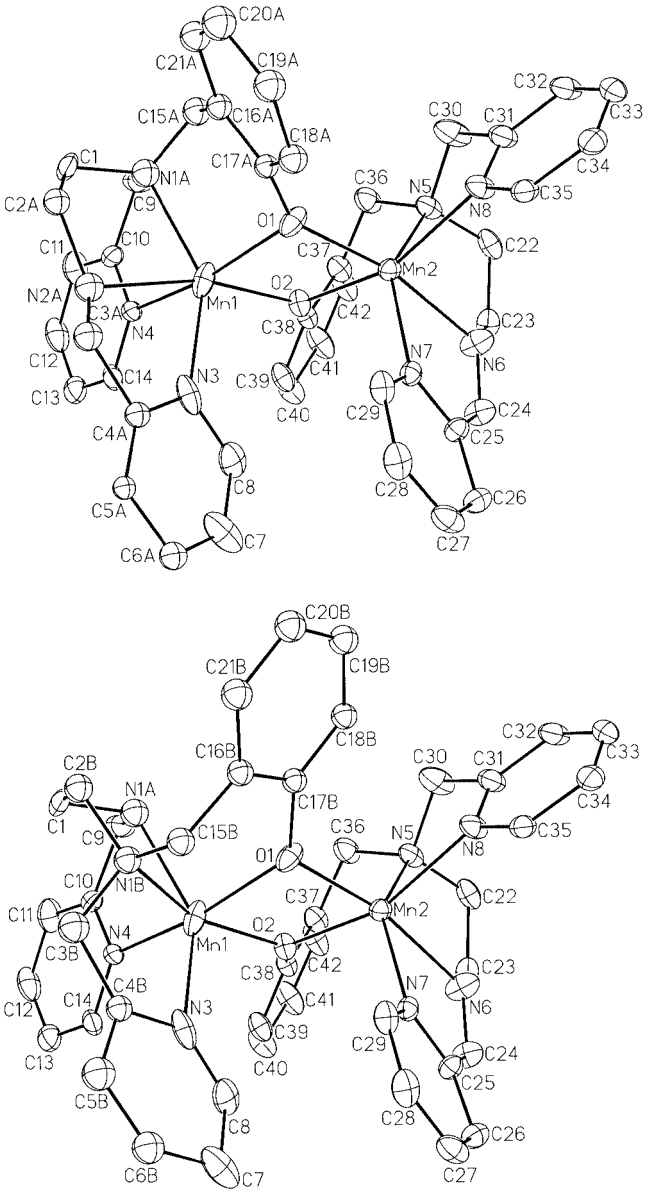

Fiugre 1. Views of the cations **1a** (top) and **1b** (bottom)

Table 1. Selected bond lengths [Å] and angles [°] for **1a** and **1b**; values are common to **1a** and **1b** unless specified

Mn1−O1	2.144(4)	Mn2−O1	2.129(4)
Mn1−O2	2.104(4)	Mn2−O2	2.103(4)
Mn1−N1A	2.278(6)	Mn2−N5	2.336(5)
Mn1−N2A (**1a**)	2.375(14)	Mn2−N6	2.279(6)
Mn1−N1B (**1b**)	2.327(10)		
Mn1−N3	2.266(7)	Mn2−N7	2.256(5)
Mn1−N4	2.284(5)	Mn2−N8	2.232(5)
O1−Mn1−N4	160.4(2)	O2−Mn2−N8	156.2(2)
N1A−Mn1−N3	144.5(2)	N5−Mn2−N7	145.7(2)
N2A−Mn1−O2 (**1a**)	164.9(3)	N6−Mn2−O1	166.9(2)
N1B−Mn1−O2 (**1b**)	156.7(3)		
Mn1−O1−Mn2	100.3(2)	Mn1−O2−Mn2	102.5(2)

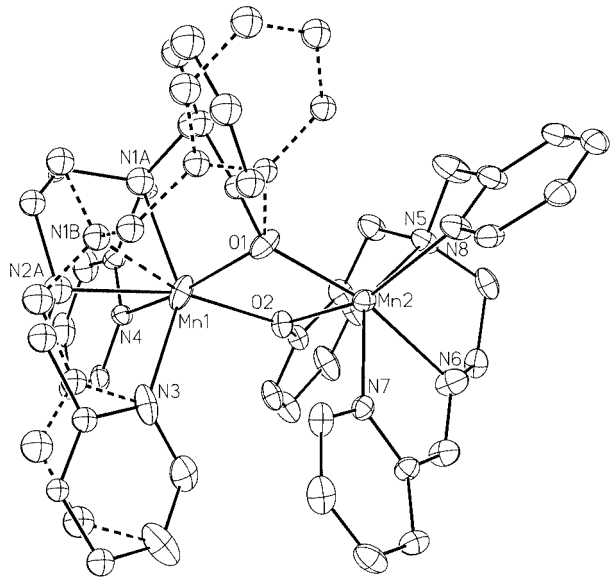

Figure 2. Comparison of the cations **1a** and **1b**, showing the differences in the Mn1 moieties; N1A of **1a** and N2B of **1b** are superimposed

atom in **1a** [N1A−Mn1−O2 113.8(2)°] while it is in the *trans* position in **1b** [N1B−Mn1−O2 156.7(3)°], (iii) the pyridine ring, slightly different in its orientation in the two Mn1 moieties, which contains the N3 atom, is linked to the imine nitrogen atom N2A atom in **1a** but to the tertiary amine N1B atom in **1b**, (iv) consequently, the two aromatic group substituents of the tertiary amine are *cis* to each other in **1b** [O1−Mn1−N3 102.7(2)°] while they are *trans* to each other in **1a** [O1−Mn1−N4 160.4(2)°] as it is around the Mn2 site [O2−Mn2−N8 156.2(2)°].

Such foldings can be compared to the ones of the same or closely related pentadentate ligands around Mn^{III} or Fe^{III} dinuclear complexes. The complexes $[L'_iMn-(\mu\text{-}O)-MnL'_i]^{n+}$ (n = 2, 3) have been characterised by X-ray crystallography.[17] The folding of the isomeric ligand L'^{-}_{i} presents the same characteristics as that of the ligand L^{-}_{i}, that is (i) the two aromatic groups anchored to the tertiary amine nitrogen atom are *trans* to each other, (ii) the tertiary amine nitrogen atom is *trans* to the group linked to the imine nitrogen atom (the phenolate ring in L'^{-}_{i}) and (iii) the imine nitrogen atom is *trans* to the exogeneous ligand. The same folding is observed for the ligand L'^{-}_{a} around the Fe^{III} ion in the complex $[L'_aFe-(\mu\text{-}O)-FeL'_a]^{2+}$,[18,19] and the secondary amine nitrogen atom in L'^{-}_{a} and the imine nitrogen atom in L'^{-}_{i} behave the same. In contrast, the ligand L^{-}_{a} adopts another folding in the complex $[L_aFe-(\mu\text{-}O)-FeL_a]^{2+}$.[18,19] The common features observed with the coordination around the Mn1 site just described in **1b** are (i) the two aromatic rings linked to the tertiary amine nitrogen atom are *cis* to each other and (ii) the tertiary amine nitrogen atom is *trans* to the extra ligand. The main difference lies in the ligation of the secondary amine nitrogen atom that is *trans* to the phenolate group. The variety of foldings observed when the ligand is in the reduced form (L^{-}_{a} and L'^{-}_{a}) compared to the unique ligating mode ob-

served when the ligand is oxidised (L_i^- and L'^-_i) is a signature of the greater flexibility when the conjugated imine function is absent.

Both Mn_2O_2 diamond core structures in **1a** and **1b** formed by the two metallic sites and the two oxygen atoms of the phenolate rings present features characteristic of such a motif. The $Mn^{II}-O$ distances (average 2.110 Å), and the $Mn^{II}-O-Mn^{II}$ bridging angles (average 101.4°) with a Mn···Mn separation of 3.280 Å, lie in the range observed for similar complexes.[20,21,25,27–34] One can note that the Mn_2O_2 diamond core structure is not planar and has a dihedral angle of 11.5°. Owing to the similarities in the Mn_2O_2 core in **1a** and **1b**, the two cations were considered identical in the following solid state studies.

Solution studies of **1** are prepared from powder samples [**1**$(ClO_4)_2$·H_2O or **1**$(BPh_4)_2$·$2CH_3COCH_3$]. One expects the same mixture of complex **1a** and **1b** observed in the crystals to exist in the powder samples and in solution.

Magnetic Susceptibility Measurements

The molar magnetic susceptibility χ_M of a powder sample of **1**$(BPh_4)_2$·$2CH_3COCH_3$ was measured as a function of temperature. The $\chi_M T$ value as a function of T is reported in Figure S1 in the Supporting Information (see also footnote on the first page of this article), together with the values obtained for **1**$(ClO_4)_2$·H_2O. For **1**$(BPh_4)_2$·$2CH_3COCH_3$, $\chi_M T$ decreases very slowly from 8.13 $cm^3 \cdot mol^{-1} \cdot K$ at 300 K to 7.91 $cm^3 \cdot mol^{-1} \cdot K$ at 100 K. Below 100 K, $\chi_M T$ decreases more rapidly to 0.9 $cm^3 \cdot mol^{-1} \cdot K$ at 2 K. This behaviour suggests a weak antiferromagnetic coupling interaction between the two high-spin Mn^{II} ions ($S_1 = S_2 = 5/2$). The best fit was obtained assuming identical parameters for the cations **1a** and **1b**: $g = 1.95$ and $J = -1.5$ cm^{-1}. These values are in agreement with those reported in the literature for complexes where two Mn^{II} ions are bridged by two phenolate ligands.[27,29,31,34]

Comparable results are obtained for **1**$(ClO_4)_2$·H_2O: $g = 1.96$ and $J = -2.9$ cm^{-1}. Small deformations of the $[Mn_2O_2]$ diamond core unit could lead to the slight differences in the g and J values determined for compound **1**, depending on the counterion.

The product of the molar magnetic susceptibility χ_M and the temperature T for a powder sample of **2**(ClO_4)·$0.5H_2O$ has a constant value of 3 $cm^3 \cdot mol^{-1} \cdot K$ from room temperature down to 30 K (see Figure S1 in the Supporting Information; see also footnote on the first page of this article). This indicates a +III oxidation state and a high-spin electronic configuration for the manganese ion ($S_{Mn^{III}} = 2$). $\chi_M T$ decreases below 30 K to reach 1.8 $cm^3 \cdot mol^{-1} \cdot K$ at 2 K. This behaviour is the signature of the zero-field splitting on the high-spin Mn^{III} ion. The best fits were obtained with a g factor close to 2 with either a positive or a negative D parameter: $g = 2.008$ and $D = +4.3$ cm^{-1} or $g = 2.006$ and $D = -4.5$ cm^{-1}. A weak intermolecular antiferromagnetic coupling between high-spin Mn^{III} ions can also contribute to the drop of $\chi_M T$ below 30 K. Mn^{III} complexes usually present an elongated octahedral geometry which corresponds to a negative D parameter.[35] The g and D values deduced here are in agreement with those determined by high-frequency EPR spectroscopy on other Mn^{III} complexes.[36–39]

EPR Spectroscopy

X-band EPR spectra of a powder sample of **1**$(BPh_4)_2$·$2CH_3COCH_3$ were recorded at several temperatures between 4.2 and 50 K using the perpendicular detection mode. The series is shown in Figure S2 in the Supporting Information (see also footnote on the first page of this article). All spectra exhibit features extending from 0 to 800 mT. Increasing temperature from 4.2 to 50 K does not affect the line positions but only their relative intensities. In addition, the signal intensity calculated as the double integral of the recorded spectrum does not follow a Curie law and reaches a maximum at 10 K.

The overall shape of the detected signals in conjunction with the deviation from the Curie law of the temperature dependence of the intensity is typical of dinuclear Mn^{II} complexes.[23,24,27,40–43] As previously reported in the literature, the complexity of the EPR spectra originating from weakly coupled dinuclear Mn^{II} complexes comes from the superposition of the signatures of the various paramagnetic spin states ($S = 1-5$) weighted by the Boltzmann distribution. Deconvolution procedures have been performed on systems presenting a relatively large antiferromagnetic exchange interaction.[44,45] In such systems, only the $S = 1$ and $S = 2$ excited spin states are sufficiently populated at low temperature to contribute to the EPR signal. In the present study, the exchange interaction is too small to allow for such an analysis.

A powder sample of the compound **1**$(ClO_4)_2$·H_2O was also tested in X-band EPR at 4.2 K and the observed spectrum is almost superimposable with the one of **1**$(BPh_4)_2$·$2CH_3COCH_3$.

The EPR was also run on frozen acetonitrile solutions of both compounds, either in the absence or in the presence of 0.1 M tetrabutylammonium perchlorate. The spectra recorded at 4.2 K present the same features as the ones detected on powder samples using the perpendicular or the parallel detection mode. This proves that the dinuclear structure of complex **1** is maintained in solution.

No X-band EPR signal was detected using the perpendicular detection mode on a powder sample of compound [**2**](ClO_4)·$0.5H_2O$. This is expected for integer spin states presenting a zero-field splitting much larger than the microwave quantum as is usually the case for monomeric Mn^{III} systems.

The EPR spectrum recorded on a freshly prepared acetonitrile solution of **2** displays a characteristic signature of **1**, together with signatures of free Mn^{II} ions (6 lines) and mixed valent $Mn^{III}Mn^{IV}$ species as impurities. These observations are the first indications that complex **2**(ClO_4)·$0.5H_2O$ is not stable in acetonitrile solution (vide infra).

Electrochemical Properties

The cyclic voltammogram of [**1**]$(ClO_4)_2 \cdot H_2O$ at 4×10^{-3} M in acetonitrile containing 0.1 M tetrabutylammonium perchlorate under argon is shown in Figure 3a. **1**$(BPh_4)_2 \cdot 2CH_3COCH_3$ was also investigated under reduction and showed similar results. The counterion BPh_4^- being easily oxidised, this sample was not investigated in the high potential ranges.

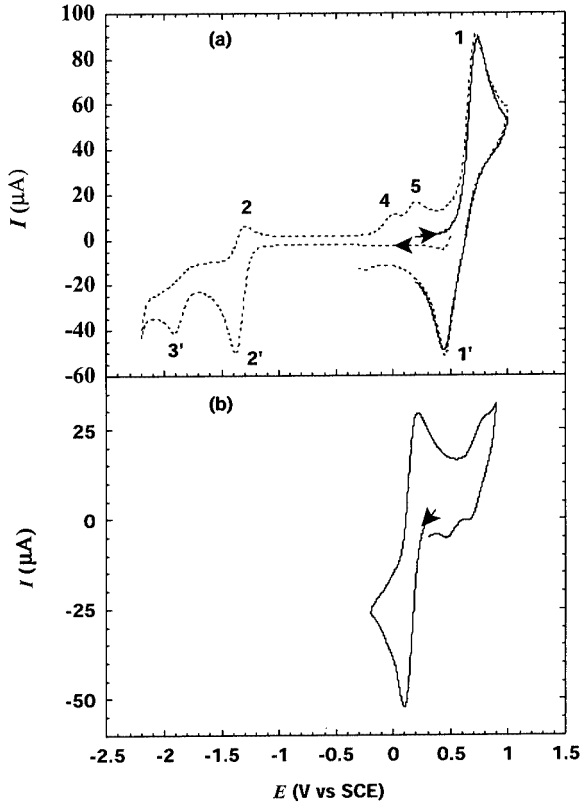

Figure 3. Cyclic voltammograms of **1**$(ClO_4)_2 \cdot H_2O$ (a) and **2**$(ClO_4)_2 \cdot 0.5H_2O$ (b) in acetonitrile containing 0.1 M of tetrabutylammonium perchlorate, $T = 20$ °C and scan rate = 100 mV·s^{-1}

The cyclic voltammetry trace of [**1**]$(ClO_4) \cdot H_2O$ shows a well-defined anodic wave (labelled wave 1 in Figure 3a) at $E_p = 0.710$ V vs. SCE, accompanied on the reverse scan by a well-defined cathodic wave (labelled 1′, $E_p = 0.450$ V vs. SCE). This oxidation process is attributed to the oxidation of the Mn^{II} ion being complexed by the imine form of the ligand in both **1a** and **1b**. This Mn^{II} oxidation potential is fairly high. $Mn^{II}Mn^{II}/Mn^{II}Mn^{III}$ oxidation potentials have been reported in the literature at about 0.35 V vs. SCE for the $[LMn_2Cl_2]$[30] or $[L'Mn_2(OAc)]^{2+}$ [46] cation where LH_2 and L′H are related to L_aH.[47] In complex **1**, the higher potential value is related to the lower number of the charged ligand around the Mn^{II} ion. A value of 0.598 V vs. SCE is reported in the literature for the $Mn^{II}Mn^{II}/Mn^{II}Mn^{III}$ oxidation potential in the case of the neutral bis(phenolato)-bridged $[Mn_2^{II}(SALPS)_2]$ dinuclear complex.[27,48] The Mn^{II} ion complexed by the amine ligand is expected to be oxidised at a higher potential. Indeed other oxidation waves are detected when scanning the potential up to 1.7 V vs. SCE. Those irreversible, ill defined cyclic voltammetry traces are attributed to oxidation of the ligand (phenolic part) and overlay with the oxidation trace of the Mn^{II} ion complexed by the amine ligand.

The cyclic voltammogram displayed in Figure 3a shows a large difference in peak potential ($\Delta E_p = 260$ mV) for wave 1/1′. This indicates that the associated electron transfer is slow. In the case of slow electron transfer, determination of n, the number of electrons involved in the redox process, is not easy. For a system undergoing irreversible charge transfer kinetics (i.e. slow electron transfer), it has been shown that $|E_p - E_{p/2}|$[49] is related to αn through Equation (1), where α is the charge transfer coefficient.[50]

$$\alpha n = \frac{0.048}{|E_p - E_{p/2}|} \quad (1)$$

In the present case, considering the symmetrical shape of the entire wave, a value of 0.5 can be taken for α. At this point one must be concerned with the influence of solution resistance since it can affect the position of the peak potential. Therefore particular care was taken to insure that the present ohmic drop was correctly compensated. From $|E_p - E_{p/2}|$ values listed in Table 2, one can establish that $n = 1$. This value was confirmed by chronocoulometry measurements. A step potential ($E = +1$ V vs. SCE, $t = 500$ ms or 250 ms) was applied to the working electrode of known surface area.[51] The chronocoulometry response gives the total charge passed Q vs. time t from the initial step. From the linear relationship[52] between Q and $\sqrt{t}$, a value of 1.2 was found for n. Thus, at the time scale of cyclic voltammetry (v range 50−500 mV·s^{-1}), or for chronocoulometry with time steps shorter than 1 s, the first oxidation step corresponds to Equation (2).

Table 2. Potential peak values and electron transfer rate constants for the $Mn^{II}Mn^{II}/Mn^{II}Mn^{III}$ oxidation in **1**$(ClO_4)_2 \cdot H_2O$

v [mV·s^{-1}]	E_{pa} [a] [V vs. SCE]	$E_{pa/2}$ [a] [V vs. SCE]	E_{pc} [a] [V vs. SCE]	ΔE_p [b] [mV]	k_s^{app} [c] [cm·s^{-1}]
50	0.705	0.595	0.460	245	7.7×10^{-4}
75	0.705	0.600	0.465	240	9.9×10^{-4}
100	0.710	0.610	0.450	260	9.4×10^{-4}
200	0.730	0.625	0.435	295	9.4×10^{-4}
300	0.730	0.625	0.445	285	1.3×10^{-3}
400	0.725	0.625	0.435	290	1.4×10^{-3}
500	0.730	0.630	0.440	290	1.5×10^{-3}
1000	0.750	0.650	0.410	340	1.4×10^{-3}

[a] E_{pa} and E_{pc} are the values of the anodic and of the cathodic peak potential, respectively, of the wave of interest. [b] ΔE_p is defined as the difference between the anodic and the cathodic peak potentials. [c] k_s^{app} is calculated according to Equation (3) given in the text with $\alpha = 0.5$, $D = 15 \times 10^{-6}$ cm$^2 \cdot$ s^{-1} and $T = 298$ K.

$$Mn^{II}Mn^{II} \rightarrow Mn^{II}Mn^{III} + e^- \quad (2)$$

It was not possible to confirm this stoichiometry by controlled potential electrolysis at $E = +1$ V vs. SCE, due to the instability of the $Mn^{II}Mn^{III}$ state on the electrolysis time

scale, even when lowering the temperature down to −30 °C. The quasi-reversibility of this oxidation step was studied by cyclic voltammetry, which showed that the peak separation, ΔE_p, for the redox couple $Mn^{II}Mn^{II}/Mn^{II}Mn^{III}$ varied between ca. 240 and 340 mV as the scan rate was increased from v = 50 to 2000 mV·s^{-1}. Table 2 gives the measured ΔE_p values for a series of voltammograms at different scan rates. Values of the apparent charge transfer rate constant (k_s^{app}) can be obtained using the procedure of Nicholson[50] for peak separations smaller than 210 mV. When ΔE_p exceeds this value, k_s^{app} [cm^{-1}] can be calculated using Equation (3), where D is the diffusion coefficient of the species of interest [cm^2·s^{-1}] and v the scan rate [m^{-1}].

$$k_s^{app} = 2.18\sqrt{\frac{D\alpha nFv}{RT}}\exp\left(\alpha^2\frac{nF}{RT}\Delta E_p\right) \quad (3)$$

Values of k_s^{app} obtained for different values of v are listed in Table 2 and a mean value of 1.2×10^{-3} cm·s^{-1} is found. This is in agreement with what is found in the literature for slow electron transfer in inorganic compounds. For example, a value of 10^{-3} cm·s^{-1} is found for the electron transfer constant of the reduction of a (porphyrin)Mn^{III} compound in dimethyl sulfoxide.[53]

This low value of the electron transfer can mainly be attributed to the fact that the oxidation process requires structural reorganisation of the original $Mn^{II}Mn^{II}$ cation. Indeed the geometry around the Mn^{III} ion should become axially distorted, due to the Jahn−Teller effect. The constraint of the structure imposed by the phenolato bridges makes this reorganisation difficult. Moreover, it was never possible to generate an $Mn^{II}Mn^{III}$ species that is stable in solution when running exhaustive electrolysis at E = +1 V vs. SCE. EPR spectra recorded on such an electrolysed solution did not show the expected $Mn^{II}Mn^{III}$ signature. Indeed, the observed signal is characteristic of monomeric Mn^{II} species, suggesting that most of the complexes remaining in solution are monomeric EPR-silent Mn^{III} entities. These observations sustain the fact that the phenolato bridges cannot support the dimeric structure in a mixed-valent state.

When scanning towards low potentials, two cathodic waves (noted as 2′ and 3′, see a in Figure 3) are observed. The first appears at E_p = −1.380 V vs. SCE and the second at −1.910 V vs. SCE. When scanning back to the oxidative potential, a first anodic wave is observed at E_p = −1.300 V vs. SCE (wave 2) and is related to the cathodic wave 2′. Scanning back towards higher potentials generates two new anodic waves (denoted 4 and 5) at E_p = 0.005 V and E_p = 0.190 V, respectively. The waves 2′ and 3′ are attributed to the [2e$^-$,1H$^+$] reductive process of the imine function of the ligand. Indeed the addition of perchloric acid to the solution results in the shift of the peak potentials towards positive values (not shown). Increasing the scan rate results in the increase of reversibility of wave 2′/2, thus showing that the reduction process associated with wave 2 generates a very reactive species. We propose this first reduced species to be an anion radical, the unpaired electron being located on the nitrogen atom of the imine part of the ligand. This very reactive anion radical is immediately protonated and further reduced at −1.910 V (wave 3′). Waves 4 and 5 are tentatively attributed to monomeric Mn^{II} species, most likely generated consecutively by the reduction process 2′ and 3′. Indeed, the monomeric **2**$(ClO_4)_2$ species exhibits an Mn^{II}/Mn^{III} redox process in the potential range of waves 4 and 5.

The cyclic voltammogram of **2**$(ClO_4)_2$·H_2O in acetonitrile containing 0.1 M tetrabutylammonium perchlorate under Ar is shown in Figure 3b. The most intense wave at $E_{1/2}$ = 0.150 V vs. SCE [$E_{1/2} = (E_{pa} + E_{pc})/2$, ΔE_p = 180 mV] is attributed to the reduction of the Mn^{III} into Mn^{II} species. This value lies between the ones measured on acetonitrile solutions of {[$py_2(NMe)_2$]$Mn^{II}Cl_2$} ($E_{1/2}$ = 0.55 V vs. SCE) and {[$py_2(NMe)_2$]$Mn^{III}F_2$}$^+$ ($E_{1/2}$ = −0.07 V vs. SCE) where $py_2(NMe)_2$ stands for *N*,*N*′-dimethyl-2,11-diaza[3,3]-(2,6)pyridinophane.[38] The fairly low value for the reduction potential of **2** agrees with the coordination of two negatively charged ligands, the phenolate and the acetate, to the Mn^{III} site. In the anodic part of the voltammogram, a second and less intense wave is observed at $E_{1/2}$ = 0.770 V and is related to the conversion of **2** into **1** (vide infra).

UV/Vis Spectroscopy

The UV/Vis spectrum of complex **2** was recorded on a freshly prepared acetonitrile solution and is reproduced in Figure 4 [curve (a)]. Three bands are found at 373 (ε = 1770 M^{-1}·cm^{-1}), 502 (940) with a shoulder at 475 (1050),

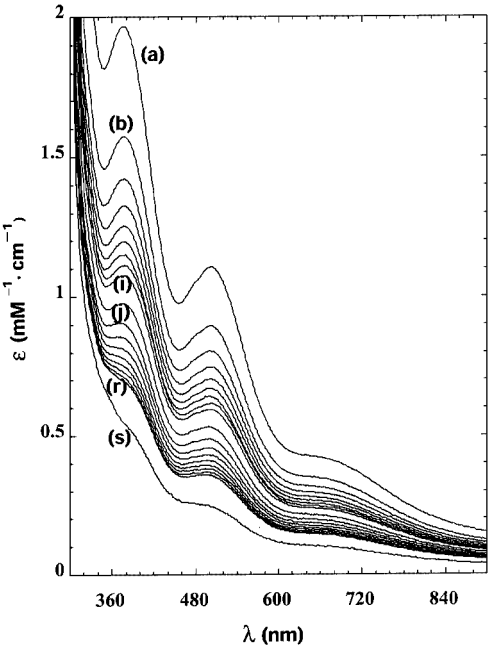

Figure 4. Time evolution of the UV/Vis spectrum of **2**$(ClO_4)_2$·0.5H_2O, 10^{-3} M in acetonitrile; spectrum (a) corresponds to the freshly prepared solution (t = 0); spectra (b) to (i) are recorded every 15 min (t = 15−120 min) and spectra (j) to (r) every hour (t = 180−660 min); spectrum (s) was recorded 46 h after spectrum (a)

and 670 nm (330). The more intense band detected in the near UV region is also observed in Mn^{III}-based complexes containing phenolato ligands and may be assigned to a phenolato-to-Mn^{III} charge transfer (LMCT) transition.[46,54,55] The last two transitions may be attributed to d-d transitions of the Mn^{III} ion according to the literature.[56,57] The low extinction coefficient measured at 670 nm enforces such an attribution. The greater absorption detected around 500 nm suggests that this band does not arise only from a d-d transition and may overlap with other LMCT bands. Resonance Raman experiments performed on dinuclear Mn^{III} complexes presenting the bis(μ-acetato)(μ-oxo) core unit suggest that the acetato-to-Mn^{III} charge transfer transition occurs in the range 450 to 500 nm rather than around 400 nm.[58] We thus propose that the absorption observed in **2** could originate from the $AcO^- \rightarrow Mn^{III}$ LMCT transition but we cannot reject a contribution from a phenolato $\rightarrow Mn^{III}$ LMCT transition.[59]

Complex **1** presents features only in the UV region [282 (ε = 2850 $cm^{-1}\cdot M^{-1}$), 262 (3960), 238 (6000) and 210 nm (15400)] associated with π-π* transitions of the ligand, in agreement with the +II oxidation state of the manganese ions.

Evolution of 2 into 1

All the attempts to obtain crystals of complex **2** ineluctably led to the formation of crystals of complex **1**. Thus, we decided to investigate the transformation of **2** into **1**, using different techniques.

A freshly prepared acetonitrile solution of **2** was allowed to evolve at room temperature and the UV/Vis spectra were recorded every 15 min. The evolution is presented in Figure 4. 36% of the initial absorption is lost in 1 h. It was not possible to interpret the series of spectra assuming the existence in solution of only two chromophores. Indeed, the band at 502 nm and the shoulder at 475 nm do not obey the same kinetic law. This implies the formation of at least one intermediate species (not identified).

The transformation was also monitored by EPR spectroscopy. As mentioned above, a signal attributed to **1** was detected on the freshly prepared acetonitrile solution of **2**, which significantly increased with time. Cyclic voltammetry and mass measurements confirmed the fast generation of **1** from **2**.

Electrospray mass spectra were recorded on freshly prepared acetonitrile solutions of complexes **1** and **2**. For complex **1**, peaks at *m*/*z* values of 901 and 903 are detected and attributed to the $\{[L_iMn^{II}Mn^{II}L_i](ClO_4)\}^+$ and $\{[L_iMn^{II}Mn^{II}L_a](ClO_4)\}^+$ entities, respectively. For complex **2**, no peak was detected at the expected *m*/*z* value of 461 for the monocationic $[L_aMn^{III}(OAc)]^+$ species. On the other hand, the above-mentioned peaks at *m*/*z* values of 901 and 903 were well observed, clearly indicating the conversion of **2** into **1** in acetonitrile solution.

Conclusion

Mn^{III} coordination chemistry has been investigated with a new pentadentate ligand L_aH with an $[N_4O]$ coordination sphere. It was expected to form a new dimeric $Mn^{III}-(\mu\text{-}O)-Mn^{IV}$ system, as has previously been obtained with an isomeric $[N_4O]$ ligand[17] (L_i'), but a mononuclear $[L_aMn^{III}]^{2+}$ complex **2** was obtained. It was found that this monomeric complex spontaneously evolves in acetonitrile solution into phenolato-bridged $Mn^{II}Mn^{II}$ dimeric complexes with the concomitant oxidation of the ligand. The formation of this bridge is made possible owing to the fairly flexible phenolate arm, when the conjugated imine function is absent in contrast to what has been observed in $[L_i'Mn-(\mu\text{-}O)-MnL_i']^{n+}$ (n = 2, 3). X-ray crystal structure analyses revealed that there is indeed a mixture of two closely related complexes: in one case both ligands L_a have been oxidised to the imine form leading to the $[L_iMn^{II}Mn^{II}L_i]^{2+}$ cation **1a**, whereas in the other only one ligand has been oxidised leading to the $[L_aMn^{II}Mn^{II}L_i]^{2+}$ cation **1b**. One can note that the oxidation of the ligand L_aH into L_iH is a $(2e^-,2H^+)$ process, while the concomitant reduction of Mn^{III} into Mn^{II} implies only one electron. We thus propose that the mononuclear complex **2** evolves in solution according to Equation (4).

$$6\ [L_aMn(OAc)]^+ \rightarrow [L_iMnMnL_i]^{2+} + [L_iMnMnL_a]^{2+} + [L_aMnMnL_a]^{2+} + 6\ OAc^- + 6\ H^+ \quad (4)$$

The three complexes would present the same bis(μ-phenolato)-bridged core unit and would be indistinguishable by EPR spectroscopy for instance. Complex $[L_aMn^{II}Mn^{II}L_a]^{2+}$ would remain in solution during the crystallisation process. Further investigation on the mechanism of this evolution was not pursued. A complete study would require controlling the pH value and the amount of acetate ions during the synthesis and crystallisation processes. In order to avoid the oxidation of the secondary amine of the L_aH ligand, methylation of the nitrogen atom has been performed. Manganese coordination chemistry of both the Mn^{II} and Mn^{III} oxidation states with this pentadentate ligand is under investigation.

Experimental Section

General Remarks: Reagents and solvents were purchased commercially and used as received. Elemental analysis: Analyses were performed by the Service Central d'Analyse du CNRS (Vernaison-France) for C, H, B, Cl, Mn, N. Infrared spectroscopy: Spectra were recorded on KBr pellets in the range of 4000 to 200 cm^{-1} with a Perkin–Elmer Spectrum 1000 spectrophotometer. The synthesis of L_aH has been described previously.[18]

Caution: *Perchlorate salts of metal complexes with organic ligands are potentially explosive. Only small quantities of these compounds should be prepared and handled behind suitable protective shields.*

Syntheses

[1](BPh$_4$)$_2$·2CH$_3$COCH$_3$: An ethanol solution (5 mL) of L_aH (348 mg, 1.0 mmol) and triethylamine (0.2 mL, 2.0 mmol) was added to an ethanol solution (5 mL) of Mn(OAc)$_3$·2H$_2$O (268 mg, 1.0 mmol) while stirring. The resulting brown solution was stirred for an extra hour and filtered at least twice in order to eliminate the remaining Mn(OAc)$_3$·2H$_2$O. To the filtrate sodium tetraphenylborate (342 mg, 1.0 mmol) was added. The brownish powder thus obtained, was then washed with ethanol, dried on a frit, and redissolved in acetone. Crystals suitable for X-ray crystallography were obtained by slow evaporation of acetone. 170 mg (ρ = 11%) of crystallised complex was collected by filtration. IR (KBr): $\tilde{\nu}$ = 3461 (w), 3254 (w), 3053 (m), 1710 (m), 1665 (s), 1597 (w), 1580 (m), 1569 (m), 1479 (w), 1453 (m), 1443 (m), 1360 (s), 1265 (w), 1220 (m), 1156 (s), 1101 (s), 1031 (s), 1015 (s), 974 (s), 882 (s), 841 (s), 751 (m), 733 (w), 706 (w), 643 (s), 624 (s), 611 (m), 581 (s), 528 (s), 470 (s), 412 (s) cm^{-1}. $C_{96}H_{95}B_2Mn_2N_8O_4$ (1556.3): calcd. C 74.09, H 6.15, B 1.36, Mn 7.06, N 7.20; found C 73.68, H 6.11, B 2.06, Mn 7.00, N 6.97.

[1](ClO$_4$)$_2$·H$_2$O: An ethanol solution (5 mL) of L_aH (348 mg, 1.0 mmol) and triethylamine (0.2 L, 2 mmol) was added to an ethanol solution (5 mL) of Mn(OAc)$_3$·2H$_2$O (268 mg, 1.0 mmol) while stirring. The resulting brown solution was stirred for several hours and filtered at least twice in order to eliminate the remaining Mn(OAc)$_3$·2H$_2$O. To the filtrate sodium perchlorate (122 mg, 1.0 mmol) was added. The pale brownish powder thus obtained, was then washed with ethanol, and dried on a frit. IR (KBr): $\tilde{\nu}$ = 3440 (s), 3278 (m), 3059 (w), 2912 (m), 1661 (w), 1595 (s), 1570 (m), 1479 (s), 1453 (m), 1442 (m), 1294 (m), 1265 (s), 1152 (m), 1094 (s), 1017 (m), 884 (w), 838 (w), 769 (m), 762 (m), 725 (w), 636 (w), 624 (w), 611 (m), 579 (w), 472 (w), 412 (w) cm^{-1}. $C_{42}H_{45}Cl_2Mn_2N_8O_{11}$ (1018.6): calcd. C 49.52, H 4.45, Cl 6.96, N 11.00; found C 49.61, H 4.63, Cl 7.33, N 10.82.

[2](ClO$_4$)·0.5H$_2$O: An ethanol solution (5 mL) of L_aH (348 mg, 1.0 mmol) was added to an ethanol solution (5 mL) of Mn(OAc)$_3$·2H$_2$O (268 mg, 1.0 mmol) while stirring. The resulting dark purple solution was stirred for 5 min and filtered at least twice in order to eliminate the remaining Mn(OAc)$_3$·2H$_2$O. To the filtrate sodium perchlorate (122 mg, 1.0 mmol) was added. The solution was stirred for an extra hour and the purple powder thus obtained, was then washed with ethanol, and dried on a frit. IR (KBr): $\tilde{\nu}$ = 3416 (s), 3148 (m), 2970 (w), 2926 (w), 1607 (w), 1568 (m), 1479 (s), 1450 (s), 1445 (s), 1428(m), 1375(s), 1327 (s), 1283 (m), 1263 (s), 1160 (w), 1088 (s), 1017 (m), 974(w), 944 (w), 930 (w), 887 (w), 852 (w), 783 (s), 765 (s) 56 (s), 724 (w), 658 (w), 640 (m), 623 (s), 584 (w), 579 (w), 415 (w) cm^{-1}. $C_{23}H_{27}ClMnN_4O_{7.5}$ (569.9): calcd C 48.48, H 4.78, Cl 6.22, N 9.83; found C 48.35, H 4.72, Cl 6.65, N 9.58.

Crystallographic Data Collection and Refinement of the Structure of [1](BPh$_4$)$_2$·2CH$_3$COCH$_3$: The crystal data of [**1**](BPh$_4$)$_2$·2CH$_3$COCH$_3$ and the parameters of data collection are summarized in Table 3. A honey-colored crystal of approximate dimensions 0.30 × 0.20 × 0.15 mm was selected. The diffraction collection was carried out with a Nonius diffractometer, equipped with a CCD detector. The lattice parameters were determined from ten images recorded with 2° Φ-scans and later refined on all data. The data were recorded at 123 K. A 180° Φ-range was scanned with 2° steps with a crystal-to-detector distance fixed at 30 mm. Data were corrected for Lorentz polarisation. The structure was solved by direct methods and refined by full-matrix least squares on F^2 with anisotropic thermal parameters for all non-H atoms. One ligand was found disordered on two positions with a 0.5 occupation factor. H atoms were introduced at calculated positions (except for atoms of the disordered ligands) and constrained to ride on their parent C atom. All calculations were performed with an O2 Silicon Graphics Station with the SHELXTL package.[60] Crystal data are summarized in Table 3. CCDC-178266 contains the supplementary crystallographic data for this paper. These data can be obtained free of charge at www.ccdc.cam.ac.uk/conts/retrieving.html or from the Cambridge Crystallographic Data Centre, 12, Union Road, Cambridge CB2 1EZ, UK [Fax: (internat.) + 44-1223/336-033; E-mail: deposit@ccdc.ac.uk].

Table 3. Crystallographic data for [**1**](BPh$_4$)$_2$·2CH$_3$COCH$_3$

Empirical formula	$C_{96}H_{95}B_2Mn_2N_8O_4$
Formula mass	1556.3
Temperature [K]	123
Wavelength [Å]	0.71073
a [Å]	24.502(5)
b [Å]	14.805(3)
c [Å]	25.626(5)
β [°]	115.86(3)
Volume [Å^3]	8365(3)
Z	4
Density [g·cm^{-3}]	1.236
μ [mm^{-1}]	0.359
θ_{max} [°]	24.69
hkl ranges	$0 \le h \le 28$ $0 \le k \le 17$ $-30 \le l \le 27$
Reflections measured	51714
Reflections independent	14126
Reflections with $I > 2\sigma(I)$	7772
Parameters	962
$R1 = \Sigma\|\|F_o\| - \|F_c\|\|/\Sigma\|F_o\|$	0.1004
$wR2 = \{\Sigma[w(F_o^2 - F_c^2)^2]^2/\Sigma w(F_o^2)^2]\}^{1/2}$ $w = 1/[\sigma^2(F_o^2) + (0.1000P)^2]$ where $P = (F_o^2 + 2F_c^2)/3$	0.2120
(Δ/σ)max	0.016
$\Delta\rho_{max}$ [e·Å^{-3}]	0.566
$\Delta\rho_{min.}$ [e·Å^{-3}]	−0.475

Magnetic Susceptibility Measurements: Magnetic susceptibility data were recorded with an MPMS5 magnetometer (Quantum Design, Inc.). The calibration was made at 298 K using a palladium reference sample furnished by Quantum Design, Inc. The data were collected over a temperature range of 2−300 K at a magnetic field of 0.5 or 1 T and were corrected for diamagnetism. In the case of **1**, the $\chi_M T$ vs. T curves were fitted using the van Vleck formula and assuming the same g factor for each spin state S. The energies appearing in the exponential arguments are derived from the Heisenberg−Dirac-van Vleck Hamiltonian $-JS_1 \cdot S_2$. The total spin S runs from $|S_1 - S_2|$ to $S_1 + S_2$ by unit steps. The fitting procedure used for complex **2** is derived from magnetisation calculations described previously.[61]

EPR Spectroscopy: EPR Spectra were recorded with a Bruker 200D spectrometer at the X-band. For low-temperature studies, an Oxford Instrument continuous-flow liquid helium cryostat and a temperature control system were used.

Cyclic Voltammetry and Chronocoulometry: Cyclic voltammetry and chronocoulometry measurements were recorded with an EGG PAR potentiostat (M273 model). The counter electrode was an Au wire, the working electrode, a glassy carbon disk, was carefully polished before each voltammogram with a 1 μm diamond paste, sonicated in an ethanol bath and then washed carefully with eth-

anol. It is worth noting that in the absence of such treatment of the working electrode surface, the successive cyclic voltammograms were not reproducible. The reference electrode was an $Ag/AgClO_4$ electrode (0.530 V vs. NHE electrode), isolated in a fritted bridge. The solvent used was distilled acetonitrile where tetrabutylammonium perchlorate was added to obtain a 0.1 M supporting electrolyte, when the experiments were carried out at room temperature, or 0.2 M, when the experiments were carried out at low temperature (below 10 °C). Low-temperature regulation was insured by a Julabo circulation cryostat.

UV/Vis Spectroscopy: UV/Vis spectra were recorded with a Cary 300 Bio spectrophotometer at 20 °C with 1-cm quartz cuvettes.

Electrospray Ionisation Ion Trap Mass Spectrometry: All experiments were performed with an ESQUIRE ion trap (Bruker-Franzen Analytic GmbH, Bremen, Germany). The used instrument has a fundamental RF frequency of 781 kHz and was used here in the *standard* mode with a mass-to-charge ratio up to 2000 Th, using a 260.3 kHz frequency as axial modulation. The ion trap operated at an uncorrected partial He buffer gas pressure of 3.4×10^{-5} Torr ($4.5\ 10^{-3}$ Pa). A differentially pumped interface transferred the ions from the electrospray source (Analytica of Brandford, Inc., Brandford, CT) to the mass spectrometer. No Ion Current Control (ICC) was used, allowing the adjustment of the ion accumulation time. Some applied parameters were unchanged for all experiments, such as the RF frequency amplitude of the hexapole (700 V), and the voltage applied on the electron multiplier (−1500 V). The dynode voltage of the electron multiplier was −5 kV, the delay before scanning 10 ms and the exit lens voltage −50 V, with the low *m/z* cutoff value at 50 Th.

Infused Solutions: The complexes were analysed in the positive-ion mode. Diluted samples (ca. 10^{-4} M) in pure acetonitrile were infused into the ESI source using a Cole−Parmer Instrument Company (74900 series) syringe pump at a flow rate of 120 μL/h. The capillary entry voltage was about −3500 V. The N_2 drying gas temperature was 150 °C with a flow rate of 200 L/h.

[1] E. J. Larson, V. L. Pecoraro, in *Manganese Redox Enzymes* (Ed.: V. L. Pecoraro), VCH Publishers, Inc., New York, **1992**, p. 1−28.
[2] R. J. Debus, *Biochim. Biophys. Acta* **1992**, *1102*, 269−352.
[3] V. K. Yachandra, K. Sauer, M. P. Klein, *Chem. Rev.* **1996**, *96*, 2927−2950.
[4] G. C. Dismukes, *Chem. Rev.* **1996**, *96*, 2909−2926.
[5] N. A. Law, M. T. Caudle, V. L. Pecoraro, *Adv. Inorg. Chem.* **1998**, *46*, 305−440.
[6] V. V. Barynin, M. M. Whittaker, S. V. Antonyuk, V. S. Lamzin, P. M. Harrison, P. J. Artymiuk, J. W. Whittaker, *Structure* **2001**, *9*, 725−738.
[7] A. Zouni, H.-T. Witt, J. Kern, P. Fromme, N. Krauß, W. Saenger, P. Orth, *Nature* **2001**, *409*, 739−743.
[8] A. W. Rutherford, P. Faller, *Trends Biochem. Sci.* **2001**, *26*, 341−344.
[9] K. Hasegawa, T.-A. Ono, Y. Inoue, M. Kusunoki, *Bull. Chem. Soc. Jpn.* **1999**, *72*, 1013−1023.
[10] J. M. Peloquin, K. A. Campbell, D. W. Randall, M. A. Evanchik, V. L. Pecoraro, W. H. Armstrong, R. D. Britt, *J. Am. Chem. Soc.* **2000**, *122*, 10926−10942.
[11] T. G. Carrell, A. M. Tyryshkin, G. C. Dismukes, *J. Biol. Inorg. Chem.* **2002**, *7*, 2−22.
[12] L. Le Pape, E. Perret, I. Michaud-Soret, J.-M. Latour, *J. Biol. Inorg. Chem.* **2002**, *7*, 445−450.
[13] P. A. Goodson, J. Glerup, D. J. Hodgson, K. Michelsen, H. Weihe, *Inorg. Chem.* **1991**, *30*, 4909−4914.
[14] Y. Frapart, A. Boussac, R. Albach, E. Anxolabéhère-Mallart, M. Delroisse, J.-B. Verlach, G. Blondin, J.-J. Girerd, J. Guilhem, M. Cesario, A. W. Rutherford, D. Lexa, *J. Am. Chem. Soc.* **1996**, *118*, 2669−2678.
[15] W. Zweygart, R. Bittl, K. Wieghardt, W. Lubitz, *Chem. Phys. Lett.* **1996**, 272−276.
[16] K.-O. Schäfer, R. Bittl, W. Zweygart, F. Lendzian, G. Haselhorst, T. Weyhermüller, K. Wieghardt, W. Lubitz, *J. Am. Chem. Soc.* **1998**, *120*, 13104−13120.
[17] O. Horner, E. Anxolabéhère-Mallart, M.-F. Charlot, L. Tchertanov, J. Guilhem, T. A. Mattioli, A. Boussac, J.-J. Girerd, *Inorg. Chem.* **1999**, *38*, 1222−1232.
[18] S. Poussereau, PhD Thesis, Université Paris-Sud,Orsay, France, **1999**.
[19] S. Poussereau, G. Blondin, E. Anxolabéhère-Mallart, T. A. Mattioli, L. Tchertanov, J.-J. Girerd, manuscript in preparation.
[20] C. Fraser, L. Johnston, A. L. Rheingold, B. S. Haggerty, G. K. Williams, J. Whelan, B. Bosnich, *Inorg. Chem.* **1992**, *31*, 1835−1844.
[21] S. C. Shoner, P. P. Power, *Inorg. Chem.* **1992**, *31*, 1001−1010.
[22] K. Yamato, I. Miyahara, A. Ichimura, K. Hirotsu, Y. Kojima, H. Sakurai, D. Shiomi, K. Sato, T. Takui, *Chem. Lett.* **1999**, 295−296.
[23] T. Howard, J. Telser, V. J. Derose, *Inorg. Chem.* **2000**, *39*, 3379−3385.
[24] I. Romero, M.-N. Collomb, A. Deronzier, A. Llobet, E. Perret, J. Pécaut, L. Le Pape, J.-M. Latour, *Eur. J. Inorg. Chem.* **2001**, 69−72.
[25] D. J. Hodgson, B. J. Schwartz, T. N. Sorrell, *Inorg. Chem.* **1989**, *28*, 2226−2228.
[26] S.-B. Yu, S. J. Lippard, I. Shweky, A. Bino, *Inorg. Chem.* **1992**, *31*, 3502−3504.
[27] D. P. Kessissoglou, W. M. Butler, V. L. Pecoraro, *Inorg. Chem.* **1987**, *26*, 495−503.
[28] S.-B. Yu, C.-P. Wang, E. P. Day, R. H. Holm, *Inorg. Chem.* **1991**, *30*, 4067−4074.
[29] E. Gallo, E. Solari, N. Re, C. Floriani, A. Chiesi-Villa, C. Rizzoli, *J. Am. Chem. Soc.* **1997**, *119*, 5144−5154.
[30] H.-R. Chang, S. K. Larsen, P. D. W. Boyd, C. G. Pierpont, D. N. Hendrickson, *J. Am. Chem. Soc.* **1988**, *110*, 4565−4576.
[31] D. Coucouvanis, K. Greiwe, A. Salifoglou, P. Challen, A. Simopoulos, A. Kostikas, *Inorg. Chem.* **1988**, *27*, 593−594.
[32] J. C. Jeffery, P. Thornton, M. D. Ward, *Inorg. Chem.* **1994**, *33*, 3612−3615.
[33] S. Theil, Y. Ratnamala, R. Chikate, F. Dahan, A. Bousseksou, S. Padhye, J.-P. Tuchagues, *Inorg. Chem.* **1997**, *36*, 6279−6286.
[34] T. C. Higgs, K. Spartalian, C. J. O'Connor, B. F. Matzanke, C. J. Carrano, *Inorg. Chem.* **1998**, *37*, 2263−2272.
[35] H. J. Gerritsen, E. S. Sabisky, *Phys. Rev.* **1963**, *132*, 1507−1512.
[36] A.-L. Barra, D. Gatteschi, R. Sessoli, G. L. Abbati, A. Cornia, A. C. Fabretti, M. G. Uytterhoeven, *Angew. Chem. Int. Ed. Engl.* **1997**, *36*, 2329−2331.
[37] J. Limburg, J. S. Vrettos, R. H. Crabtree, G. W. Brudvig, J. C. De Paula, A. Hassan, A.-L. Barra, C. Duboc-Toia, M.-N. Collomb, *Inorg. Chem.* **2001**, *40*, 1698−1703.
[38] R. Carina, B. Albela, C. Policar, S. Poussereau, J. Cano-Boquera, J. Guilhem, L. Tchertanov, S. Un, G. Blondin, M. Delroisse, J.-J. Girerd, manuscript in preparation.
[39] A. Marvilliers, PhD Thesis, Université Paris-Sud, Orsay, France, **1999**.
[40] E. J. Laskowski, D. N. Hendrickson, *Inorg. Chem.* **1978**, *17*, 457−470.
[41] H. Adams, N. A. Bailey, N. Debaeker, D. E. Fenton, W. Kanda, J.-M. Latour, H. Okawa, H. Sakiyama, *Angew. Chem. Int. Ed. Engl.* **1995**, *34*, 2535−2537.
[42] B. E. Schultz, B.-H. Ye, X.-Y. Li, S. I. Chan, *Inorg. Chem.* **1997**, *36*, 2617−2622.
[43] B. Albela, M. Corbella, J. Ribas, I. Castro, J. Sletten, H. Stoeckli-Evans, *Inorg. Chem.* **1998**, *37*, 788−798.

[44] S. V. Khangulov, P. J. Pessiki, V. V. Barynin, D. E. Ash, G. C. Dismukes, *Biochemistry* **1995**, *34*, 2015−2025.
[45] A. E. Meier, M. M. Whittaker, J. W. Whittaker, *Biochemistry* **1996**, *35*, 348−360.
[46] H. Diril, H.-R. Chang, M. J. Nigles, X. Zhang, J. A. Potenza, H. J. Schugar, S. S. Isied, D. N. Hendrickson, *J. Am. Chem. Soc.* **1989**, *111*, 5102−5114.
[47] LH_2 is the Schiff base condensation of 2 mol of 1,3-diaminopropane with 2 mol of 4-*tert*-butyl-2,6-diformylphenol; L′H is 2,6-bis[bis(2-pyridylmethyl)aminomethyl)-4-methylphenol, also called BPMPH.
[48] $SALPS^{2-}$ is the *N*,*N*′-[1,1′-dithiobis(phenylene)]bis(salicylidene)aminato ligand.
[49] E_p is the peak potential of the considered wave and $E_{p/2}$ the potential value at half the intensity of the peak current. Both potential are expressed in V.
[50] R. S. Nicholson, I. Shain, *Anal. Chem.* **1964**, *36*, 706−723.
[51] The surface *S* of the working electrode was measured by cyclic voltammetry and chronocoulometry on a known concentration of ferrocene in acetonitrile assuming a diffusion coefficient $D = 2.3 \cdot 10^{-5}$ $cm^2 \cdot s^{-1}$.
[52] A plot of *Q* vs. $t^{1/2}$ transforms the data into a linear relationship whose slope is $2nSFC(D/\pi)^{1/2}$ where *F* is the Faraday constant and *C* the concentration.
[53] K. M. Kadish, M. Sweetland, J. S. Cheng, *Inorg. Chem.* **1978**, *17*, 2795−2797.
[54] J. A. Bonadies, M. J. Maroney, V. L. Pecoraro, *Inorg. Chem.* **1989**, *28*, 2044−2051.
[55] M. G. Patch, C. J. Carrano, *Inorg. Chim. Acta* **1981**, *56*, L71.
[56] T. S. Davies, J. P. Fackler, M. J. Weeks, *Inorg. Chem.* **1968**, *7*, 1994−2002.
[57] R. Dingle, *Acta Chem. Scand.* **1966**, *20*, 33−44.
[58] J. E. Sheats, R. S. Czernuszewicz, G. C. Dismukes, A. L. Rheingold, V. Petrouleas, J. Stubbe, W. H. Armstrong, R. H. Beer, S. J. Lippard, *J. Am. Chem. Soc.* **1987**, *109*, 1435−1444.
[59] A. Neves, S. M. D. Erthal, I. Vencato, A. S. Ceccato, Y. P. Mascarambas, O. R. Nascimento, M. Hörner, A. A. Batista, *Inorg. Chem.* **1992**, *31*, 4749−4755.
[60] G. M. Sheldrick, *SHELXTL: Program for the Refinement of Crystal Structures*, University of Gottingen, Germany, **1993**.
[61] O. Horner, E. Rivière, G. Blondin, S. Un, A. W. Rutherford, J.-J. Girerd, A. Boussac, *J. Am. Chem. Soc.* **1998**, *120*, 7924−7928.

Received January 22, 2002
[I02037]